Original paper

Establishment of local geodetic networks based on least-squares adjustments of GNSS baseline vectors

Gabriel Weiss[1], Slavomir Labant[1]*, Juraj Gasinec[1], Hana Stankova[2], Pavel Cernota[2], Erik Weiss[3], Roland Weiss[3]

[1]Technical University of Kosice, Kosice, Slovakia
e-mail: gabriel.weiss@tuke.sk; ORCID: http://orcid.org/0000-0002-1287-5408
e-mail: slavomir.labant@tuke.sk; ORCID: http://orcid.org/0000-0002-0666-4268
e-mail: juraj.gasinec@tuke.sk; ORCID: http://orcid.org/0000-0002-9060-7185

[2]VSB – Technical University of Ostrava, Ostrava, Czech Republic
e-mail: hana.stankova@vsb.cz; ORCID: http://orcid.org/0000-0003-0013-3666
e-mail: pavel.cernota@vsb.cz; ORCID: http://orcid.org/0000-0001-5537-5932

[3]University of Economics in Bratislava, Bratislava, Slovakia
e-mail: erik.weiss@euba.sk; ORCID: http://orcid.org/0000-0002-3930-7910
e-mail: roland.weiss@euba.sk; ORCID: http://orcid.org/0000-0001-5381-2369

*Corresponding author: Slavomir Labant, e-mail: slavomir.labant@tuke.sk

Abstract: Slope deformations, i.e., all types of landslides of rock masses (flow, creep, fall down, etc.), caused by gravitational forces, are the most widespread implementation of geological hazards and a negative geomorphological phenomenon that threatens the security of the population, destroy all utility values of the affected regions, negatively affects the environment, and cause considerable economic damage. Nowadays, the Global Navigation Satellite Systems (GNSS) provide accurate data for precise observations around the world due to the growing number of satellites from multiple operators, as well as more powerful and advanced technologies and the implementation of mathematical and physical models more accurately describing systematic errors that degrade GNSS observations such as ionospheric, tropospheric, and relativistic effects or multipath. The correct combination of measurement methods provides even more precise, i.e., better measurement results or estimates of unknown parameters. The combination of measurement procedures and their significant evaluations represent the essential attribute of deformation monitoring of landslides concerning the protection of the environment and the population's safety in the interest areas for the sustainable development of human society. This article presents the establishment and use of a local geodetic network in particular local space for various needs. Depending upon the specific conditions, it is possible to use GNSS technology to obtain accurate observations and achieve the results applicable to the deformation survey for subsequent processing of the adjustment procedure.

1. Introduction

The establishment of a long-term stable local geodetic network (LGN) is a condition of its use for precise geodetic activities realized in stages, including deformation monitoring of the given area's stability. The instability of a territorial unit is caused mainly by slope deformations, which are one of the most important geological factors with a direct negative impact on the environment. The most common causes of landslides can be the undercutting of the heel of the slope, the reduction of the soil strength in shear, increase in humidity, or increase of the pressure in the groundwater of the soil layers with very low permeability. Landslides are caused by the overloading of embankments, shocks, or vibrations, but also by changes in climatic conditions, especially extreme precipitation. Slope deformations also harm the sustainable development of human society, property protection, and the security of the population, contributing to economic damage.

When monitoring landslides, it is necessary to comprehensively control geological and morphological physical factors, including human activity (Pu et al., 2015). Physically-based subsurface hydrological models are frequently integrated with slope stability analysis methods to estimate which areas are susceptible to landslides (Zhou et al., 2014). The minimum bases for making good landslide forecasts are (Baum and Godt, 2010):

1. Landslide hazard maps to indicate what areas are at risk;
2. Antecedent groundwater or soil moisture levels needed for landslide occurrence;
3. Rainfall intensity and duration, which are necessary for landslide initiation;
4. Real-time meteorological data and forecasts.

Landslide warning systems provide sufficient lead time to implement actions to protect persons or property (Capparelli and Tiranti, 2010). Yune et al. (2010) analyzed rainfall-induced landslides and confirmed that landslides are caused by short-term rainfall and influenced by antecedent rainfall. Therefore, it is necessary to determine rainfall thresholds, which predict the occurrence of landslides due to antecedent rainfall (Hong et al., 2018). The frequency of monitoring depends on the expected shift, the actual shift, and the amount of previous and current precipitation. The entire landslide area, including the head, main body, and foot of landslides, needs to be monitored. The monitoring results need to provide the magnitude of the spatial changes over the monitoring period. The higher the quality of the LGN determination, the higher the reliability of such results. Accurate prediction of landslide occurrence and monitoring and early warning for ground movements are essential tasks to reduce the damages and losses caused by landslides (Chae et al., 2017).

Several deformation monitoring techniques are currently available depending on the required accuracy, extent, and nature of the observed artificial, natural objects or areas. These techniques are traditionally divided into geodetic and non-geodetic. The group of geodetic measuring techniques consists of conventional methods (precise levelling, methods based on accurate observation of angles and lengths), satellite methods (GNSS, InSAR), terrestrial, aerial photogrammetry, and LiDAR (Ge et al., 2007; Tofani et al., 2013; Pu et al., 2015; Bakon et al., 2017; Hong et al., 2018, Ma et al., 2020). These methods must have a network of points with exact spatial coordinates to verify the location

for possible use as a ground control point. For this reason, the establishment of accurate geodetic networks is essential and still actual. InSAR uses a pair of radar images acquired at different times and from different satellite positions, identifying them and evaluating the changes that have occurred in this time interval. Before deformation monitoring, it is necessary to draw up a project of all works in which the principles, methods, and timing of the individual subactivities are required to obtain reliable results given for the area concerned (Sabova and Pukanska, 2007; Wang et al., 2018). Each monitoring network is established on a unique project, in which optimal coordinate system (zero-order design), optimal configuration (first-order design), and optimal observation weights and their type (second-order design) are determined. The project guarantees that the built network of reference points allows determining the 1D, 2D, or 3D displacements on observed points at the prescribed significance level. If the projected accuracy of the network points is not achieved, an analysis is needed to re-evaluate and put in additional observations (possibly also points) and increase their weight (third-order design). When designing a project, it is necessary to use project management tools to make partial steps more efficient (Drabikova, 2016). The establishment of LGNs is currently relatively well known in the research area (Weiss et al., 2009) and used in practice. The use of the specified procedure of establishing a quality LGN has several advantages compared to the methods mentioned above, for example, accuracy, speed, and repeatability of determining the unknown parameters, and the economic and time availability of measurements and processing of results.

The monitoring aims to identify the deformation vector of observed (object) points, which represents: the movement (displacements, subsidences, and uplift of individual points) of the monitored landslide (Kukucka, 2013), undermined territory (Grecea et al., 2012; Jing et al., 2018), construction or industrial building (Manap and Voulvoulis, 2016), filling up the tailing ponds (Sun et al., 2018) or water dams (Popa and Palamariu, 2012; Gasinec et al., 2019; Ma et al., 2020). In monitoring the stability of water dams, GIS tools can use to assess the economic impacts of potential hydrological extremes (Gergelova et al., 2012; Zelenakova et al., 2015; Zelenakova et al., 2018). In the event of a crisis, eight factors that need to emphasize when dealing with the crisis have identified (Tej et al., 2015). By strain analysis of the deformation vector, more detailed conclusions about the deformation, i.e. dilatation (expansion, compression), rotation, shear, or tensile deformation of a territorial unit, as well as the prediction of their future movements, can be made (Kolcun and Sutti, 2000; Tzenkov and Gospodinov, 2003). It can apply to dams and levees, reinforced walls and slopes, excavations, and open-pit mines (Sun et al., 2018; Labant et al., 2020), roads, bridges and embankments, groundwater, ground freezing, and climate change (Chan et al., 2018), earthquake deformation. The results of strain analysis can provide decisive conclusions. Early signaling can inform of impending dangers that may have an impact on economic harm, human safety, the stability of sustainable social development, and environmental protection (Qian et al., 2012).

The advantages of using GNSS technology are mainly real-time positioning, high reliability of measurements, independence from the seasons, time of observation, or direct visibility between points (Hefty and Husar, 2007). The most important factors

affecting the accuracy of determination of the position: the duration of the measurement interval; the length of the measured baseline; the method of processing; the number of visible satellites; their geometric configuration concerning the measured points; the models used; the ambiguity solution; the type of the receiver and the antenna; the type of satellite ephemeris; as well as the degree of elimination of systematic errors (ionospheric and tropospheric refraction, incomplete knowledge of the satellites – ephemeris; atomic clock error on satellites; antenna phase variations; multipath (Schonemann et al., 2011; Jadviscok et al., 2016)).

It is necessary to assess the influence of the input parameters in the network processing and then to investigate the changes in the position of the observed points (Weiss et al., 2010; Weiss et al., 2018), whether the differences are only a result of the accumulation of measurement errors, or a change of position indicating the deformation of the network. The observed points mounted on the object (in the area) have to be observed from reference points mounted in regions without the effects of deformation (Weiss and Jakub, 2007). Each country has built geodetic point fields with varying structures, densities, and functions, which were created by applying classical astronomical, geophysical, and conventional measurement methods, using the current satellite systems. GNSS technology for geodetic applications allows each country to build homogenous geodetic structures (planar, vertical, and spatial systems) compatible with analogous systems in neighboring countries.

The majority of countries worldwide have built geodetic bases using either "classical" conventional methods in the past. E.g., in Slovak Republic (SR), the two-dimensional projected coordinate system is the "Datum of Uniform Trigonometric Cadastral Network" (D-UTCN – Krovak's projection with x southing and y westing values), the vertical system is "Baltic Vertical Datum – After Adjustment" (BVD-AA) (STN EN ISO 19111). Krovak's projection is a double conformal cartographic projection of Bessel's ellipsoid (1841) first on a reduced sphere and from the sphere to the oblique tangent cone. The x-axis forms the fundamental meridian of 42° 30 east of the Ferro meridian. The beginning of the rectangular planar coordinate system is at the apex of the cone. The x-coordinates increase to the south and the y-coordinates to the west. Or, due to the international interconnectedness of scientific, research, and technical matters, the European regional coordinate system, known as the European Terrestrial Reference System (ETRS 89), is being actively built and maintained (Hoffmann-Wellenhof et al., 2008; Kadaj, 2016). In such circumstances, in the SR, with the standard feasibility of both coordinate systems, D-UTCN and ETRS 89, for determination of the spatial position of points, mainly locally, there is also the possibility to establish a local geodetic point field with the necessary structure depending upon its function. The submitted report details the establishment and use of an LGN, particularly local space (LS), for various building needs concerning sustainable development, population safety, environmental protection, and ecological stability. Depending upon specific conditions, it is possible (within the creation of geodetic documentation for a particular building, field, and other purposes) to use GNSS technology and solutions or in combination with conventional geodetic measurements, depending upon the situation or usefulness.

In LS, it could be supposed that there are already several points documented in the state database, with coordinates from the D-UTCN, BVD-AA systems and ETRS 89 (points located outside the LS borders). Other "new" actual points will relocate if necessary, i.e. from the viewpoint of the project managers and contractors of local building work. Existing LS points (in D-UTCN, BVD-AA and ETRS systems) naturally contain necessary and useful data for identification in the state database:

1. for points in ETRS89; the epoch (e.g., 2017.0):
   – ellipsoidal (geodetic) coordinates φ, λ, h in a geographic coordinate reference system with their a priori standard deviation σ_φ, σ_λ, σ_h;
   – Cartesian coordinates in a geocentric coordinate reference system X, Y, Z with their a priori standard deviation σ_X, σ_Y, σ_Z;
2. for points in D-UTCN and BVD-AA:
   – Cartesian coordinates x, y in a geodetic datum D-UTCN (of the Krovak's projection with x southing and y westing values) with their a priori standard deviation σ_x, σ_y;
   – gravity-related (Molodensky's normal) height H with a priori standard deviations σ_H, which are feasible when implementing the given tasks.

The given report will include methods of measurement and evaluation for partial and final results from the viewpoint of required quality and reliability of the point field with the application of both coordinate systems for determination of ETRS point coordinates in the LS.

2. Establishment of a point field in the local space of the area

Taking into account the density of the point field in SR, it is also possible to assume that in the LS of interest, for implementation of project works (building and related works), there will already be several points of the state geodetic point field, e.g. points A_i, $(i = 1, 2, 3)$ (Fig. 1) with the necessary properties and appropriate data. To create
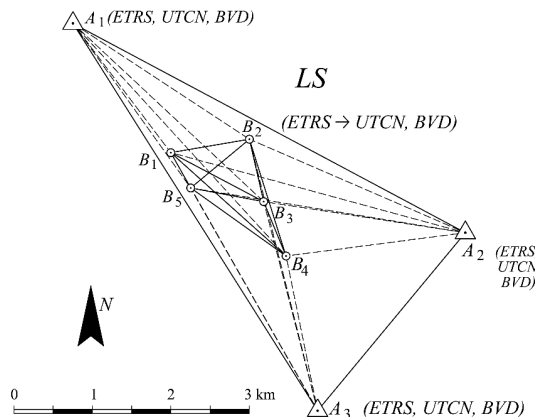

Fig. 1. Geodetic point field in local space, where A_1, A_2, A_3 are existing points, and B_1, B_2, B_3, B_4, B_5 are established points of LGN

the required suitable point structure in LS for the planned building works (i.e. ground, building, leveling, etc.), it is always necessary to establish additional geodetic points. For example, in the given case, points B_j, $(j = 1, 2, 3, 4, 5)$ (Fig. 1) located following the requirements of the project manager and field conditions so that the building of all LS objects could be correctly geodetically treated.

Mainly from the aspect of speed and quality when determining the coordinate locations of points B_j, survey, and determination of the coordinates of these points together with data on their quality, GNSS technology is generally currently preferred due to its various significant advantages compared to conventional measurement technologies.

Together with their coordinates and other parameters, the "reference" points A_i located in LS are documented in official databases: "Survey control point data" in Geodesy, Cartography and Cadastre Authority of Slovak Republic (GCCA SR) Bratislava for GNSS and conventional measurement with their pertinent or necessary utility.

Currently established "new" points B_j in LS should be precisely determined in the ETRS system, mainly taking into account their coordinates, i.e., with acceptable accuracy concerning the reliability and accuracy of the points A_i. This requirement is usually evaluated within the quality analysis of currently established points B_j, mainly based on their standard coordinate deviations $B_j(s_{\widehat{X}}, s_{\widehat{Y}}, s_{\widehat{Z}})$.

3. Results GNSS measurement of new points B_j on local space

3.1. Survey of vector structure of LGN with points A_i and B_j

The vector $d_{AiBj} = (\Delta X, \ \Delta Y, \ \Delta Z)_{AiBj}^T$ and its variance-covariance matrix:

$$\mathbf{\Sigma}_{\mathbf{AiBj}}^{(k)} = \widehat{M}_0^{2(k)} \mathbf{Q}_{\mathbf{AiBj}}^{(k)} = \widehat{M}_0^{2(k)} \begin{pmatrix} q_{\Delta X} & q_{\Delta X \Delta Y} & q_{\Delta X \Delta Z} \\ q_{\Delta Y \Delta X} & q_{\Delta Y} & q_{\Delta Y \Delta Z} \\ q_{\Delta Z \Delta X} & q_{\Delta Z \Delta Y} & q_{\Delta Z} \end{pmatrix}^{(k)} , \tag{1}$$

are the results of post-processing of simultaneous observations at the endpoints of baseline A_i, B_j (Fig. 2) in the appropriate software within the process generally denoted as GNSS Relative Static Positioning. The cofactor matrix $\mathbf{Q}_{\mathbf{AiBj}}^{(k)}$ of k-th observed vector, as well as the standard deviation $\widehat{M}_0^{(k)}$, are determined from the equations of double-differences observations, which represent the linear functions of the observed carrier phases (Leick, 2004; Hefty and Husar, 2007).

Observations of LGN points were performed by dual-frequency GNSS receivers from Leica, so post-processing of raw data was performed in Leica Geo Office software. Precise ephemeris, 15° elevation mask, satellites with longer and uninterrupted signal reception, duration of observations met the condition 20 min + 2 min/km, PDOP value < 2, etc. were used for processing. Only vectors with the fixed solutions of the ambiguities were used in the LSM processing. The vector post-processing reports are converted into the corresponding vectors and matrices for LS network adjustment.
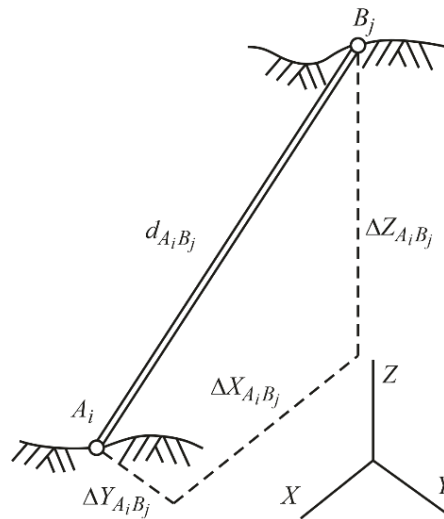
Fig. 2. Vector $d_{A_i B_j}$ (spatial distance) with its components ΔX, ΔY, ΔZ in the geocentric
Cartesian coordinate system $(X,\ Y,\ Z)$

3.2. Adjustment of the LGN with established points B_j

Based on the redundant GNSS observations at the new stabilized points B_j in LS, i.e. 3D vectors between points A_i and B_j (as well as between individual points B_j), the ETRS coordinates and their stochastic characteristics are determined using an appropriate adjustment method.

Depending upon the given situation or the requirements of various adjustment methods, it is suitable to apply those estimation methods (models), which will provide data on the primary or additional properties of the determined point field from the viewpoint of their quality.

Therefore, to obtain reliable characteristics of various outputs from adjustment methods, it is suitable to use solutions with appropriate verified models, for example:

– Gauss–Markov model (GMM) of full-rank with the minimum (necessary) or with a general number of A_i-points coordinates used for the datum network fixation in the A_i-points coordinate system;
– GMM not of full rank with minimum or general number of conditional equations relating to the estimates of the adjusted coordinates;
– Gauss–Helmert model with other suitable solutions.

Different modified approaches are massively applied for solving and determining point coordinates for various standards and exceptional situations of point fields. These are mainly solutions based on robust estimation together with the use of their suitable modifications (Caspary, 2000; Jager et al., 2005; Gasincova and Gasinec, 2010; Labant et al., 2011; Banas and Ligas, 2014).

In the given point structure of LGN (Fig. 1), the LSM estimates $B_j(\widehat{X}, \widehat{Y}, \widehat{Z})$ of the ETRS system, as well as their covariance $\Sigma_{\widehat{C}\mathbf{j}}$ and cofactor $\mathbf{Q}_{\widehat{C}\mathbf{j}}$ characteristics, will be obtained by determining the coordinates of points B_j, ($j = 1, 2, 3, 4, 5$).

In addition to the standard Least Squares Method (based on the L^2 – Euclidean norm of the residuals vector), several adjustment methods have been developed and successfully applied that are robust to potential gross errors and outliers in the observation sets.

The most common robust methods used in surveying and geodetic practice are based on linear programming techniques applied to the L^1 (Manhattan) or L^∞ (Chebyshev) of L^P norm of residuals. Attention should also be paid to Iteratively Reweighted Least Squares (IRLS) methods, based on finding estimates of the Maximum Likelihood Estimates of a generalized linear model (M-estimators), which are widely used for their simplicity. Let us mention at least some better-known of these: Huber (1964), Hampel (1980), Hekimoglu (2005), Gasinec and Gasincova (2016), the Danish method introduced by Krarup and Kubik (1983).

For estimates of point coordinates B_j and their standard deviations obtained, for example, from a conventional adjustment method: GMM of the full rank, standard components will be used for the required input and output values of the measured variables:

$$
\begin{aligned}
&\mathbf{A} && \text{– LGN configuration matrix;} \\
&\Sigma_{\mathbf{L}(k,k)} && = \operatorname{diag}\left(\Sigma_{\mathbf{L}}^{(1)} \ \Sigma_{\mathbf{L}}^{(2)} \ \cdots \ \Sigma_{\mathbf{L}}^{(k)}\right) - k \times k \text{ variance-covariance matrix} \\
& && \text{of observed vectors in which diagonal } 3 \times 3 \text{ submatrices } \Sigma_{\mathbf{L}}^{(1)}, \\
& && \Sigma_{\mathbf{L}}^{(2)}, \cdots \Sigma_{\mathbf{L}}^{(k)} \text{ are related to equation (1);} \\
&\mathbf{Q_L} && \text{– cofactors matrix of observed vectors;} \\
&\mathbf{N = A}^T \mathbf{Q_L^{-1} A} && \text{– matrix of normal equation coefficients;} \\
&\mathbf{L} && \text{– vector of observed vector components } \Delta X, \Delta Y, \Delta Z \text{ of the} \\
& && \text{baseline between all points;} \\
&\mathbf{L}^\circ && \text{– vector of approximate values of } \mathbf{L}; \\
&\mathbf{dL = L - L}^\circ && \text{– vector of reduced values of } \mathbf{L}; \\
&\widehat{\mathbf{C}} && \text{– vector of estimate of coordinates points } B_j; \\
&\mathbf{C}^\circ && \text{– vector of approximate values of coordinates points } B_j; \\
&\mathbf{d}\widehat{\mathbf{C}} = \widehat{\mathbf{C}} - \mathbf{C}^\circ && \text{– vector of adjusted coordinate complements to values } \mathbf{C}^\circ; \\
&\mathbf{V = Ad}\widehat{\mathbf{C}} - \mathbf{dL} && \text{– vector of residuals (correction of observed values of } \mathbf{L}); \\
&\sigma_0^2 && \text{– a priori variance factor.}
\end{aligned}
$$

(2)

There are several strategies for determining the a priori standard deviation of unit weight σ_0 of GNSS baselines. In common cases, it can be determined according to the relationship $\sigma_0 = a + b\, D$ ppm for the GNSS baseline standard deviation. Worldwide accepted values for static relative positioning are $a = 5$, $b = 1$, D denotes length of unit baseline.

For the expression and properties of coordinate estimates $\widehat{\mathbf{C}}_{\mathbf{Bj}}$, the stated components create the following equations:

$$\begin{aligned}
\widehat{\mathbf{C}}_{\mathbf{Bj}} &= \mathbf{C}^\circ + \mathbf{d}\widehat{\mathbf{C}} \\
&= \mathbf{C}^\circ + (\mathbf{A}^T \mathbf{Q}_{\mathbf{L}}^{-1}\mathbf{A})^{-1}\mathbf{A}^T \mathbf{Q}(\mathbf{L} - \mathbf{L}^\circ) \\
&= \mathbf{C}^\circ + \mathbf{N}^{-1}\mathbf{A}^T \mathbf{Q}_{\mathbf{L}}^{-1}\mathbf{dL},
\end{aligned} \tag{3}$$

For the cofactor matrix:

$$\mathbf{Q}_{\widehat{\mathbf{C}}} = \mathbf{N}^{-1} = (\mathbf{A}^T \mathbf{Q}_{\mathbf{L}}^{-1}\mathbf{A})^{-1}, \tag{4}$$

and for the covariance matrix of coordinate estimates:

$$\mathbf{\Sigma}_{\widehat{\mathbf{C}}} = s_0^2 \mathbf{Q}_{\widehat{\mathbf{C}}} = s_0^2 (\mathbf{A}^T \mathbf{Q}_{\mathbf{L}}^{-1}\mathbf{A})^{-1}, \tag{5}$$

where:

$$s_0^2 = \frac{\mathbf{V}^T \mathbf{Q}_{\mathbf{L}}^{-1}\mathbf{V}}{(n - k)} \tag{6}$$

is an a posteriori variance factor

n – number of measured variables i.e. the number of observed vectors times 3;

k – number of determining variables i.e. the number of determined points B_j times 3;

$n - k$ – network redundancy.

The cofactor matrix $\mathbf{Q}_{\widehat{\mathbf{C}}_{\mathbf{j}}}$ and covariance matrix $\mathbf{\Sigma}_{\widehat{\mathbf{C}}_{\mathbf{j}}}$ in the assessment of measurement quality and the processing of LGN, i.e. in the determination of point coordinates $B_j (j = 1, 2, 3, 4, 5)$, have the following solution in the given structure:

– the cofactor matrix of coordinate estimates:

$$\mathbf{Q}_{\widehat{\mathbf{C}}_{\mathbf{j}}}_{(15,15)} = \begin{pmatrix}
\mathbf{Q}_{\widehat{\mathbf{C}}\mathbf{1}} & \mathbf{Q}_{\widehat{\mathbf{C}}\mathbf{12}} & \cdots & \cdots & \mathbf{Q}_{\widehat{\mathbf{C}}\mathbf{15}} \\
\mathbf{Q}_{\widehat{\mathbf{C}}\mathbf{21}} & \mathbf{Q}_{\widehat{\mathbf{C}}\mathbf{2}} & & & \\
\vdots & & \mathbf{Q}_{\widehat{\mathbf{C}}\mathbf{3}} & & \\
\vdots & & & \mathbf{Q}_{\widehat{\mathbf{C}}\mathbf{4}} & \\
\mathbf{Q}_{\widehat{\mathbf{C}}}\mathbf{51} & & & & \mathbf{Q}_{\widehat{\mathbf{C}}\mathbf{5}}
\end{pmatrix} =$$

$$\left(\begin{array}{ccc|ccc|c|c|c}
q_{\widehat{X}1} & q_{\widehat{X}1\widehat{Y}1} & q_{\widehat{X}1\widehat{Z}1} & q_{\widehat{X}1\widehat{X}2} & q_{\widehat{X}1\widehat{Y}2} & q_{\widehat{X}1\widehat{Z}2} & \cdots & & \\
q_{\widehat{Y}1\widehat{X}1} & q_{\widehat{Y}1} & q_{\widehat{Y}1\widehat{Z}1} & q_{\widehat{Y}1\widehat{X}2} & q_{\widehat{Y}1\widehat{Y}2} & q_{\widehat{Y}1\widehat{Z}2} & & & \\
q_{\widehat{Z}1\widehat{X}1} & q_{\widehat{Z}1\widehat{Y}1} & q_{\widehat{Z}1} & q_{\widehat{Z}1\widehat{X}2} & q_{\widehat{Z}1\widehat{Y}2} & q_{\widehat{Z}1\widehat{Z}2} & & & \\
\hline
q_{\widehat{X}2\widehat{X}1} & q_{\widehat{X}2\widehat{Y}1} & q_{\widehat{X}2\widehat{Z}1} & q_{\widehat{X}2} & q_{\widehat{X}2\widehat{Y}2} & q_{\widehat{X}2\widehat{Z}2} & & & \\
q_{\widehat{Y}2\widehat{X}1} & q_{\widehat{Y}2\widehat{Y}1} & q_{\widehat{Y}2\widehat{Z}1} & q_{\widehat{Y}2\widehat{X}2} & q_{\widehat{Y}2} & q_{\widehat{Y}2\widehat{Z}2} & & & \\
q_{\widehat{Z}2\widehat{X}1} & q_{\widehat{Z}2\widehat{Y}1} & q_{\widehat{Z}2\widehat{Z}1} & q_{\widehat{Z}2\widehat{X}2} & q_{\widehat{Y}2\widehat{Z}2} & q_{\widehat{Z}2} & & & \\
\hline
& & & & & & \mathbf{Q}_{\widehat{\mathbf{C}}\mathbf{3}} & & \\
\hline
& & & & & & & \mathbf{Q}_{\widehat{\mathbf{C}}\mathbf{4}} & \\
\hline
& & & & & & & & \mathbf{Q}_{\widehat{\mathbf{C}}\mathbf{5}}
\end{array}\right), \tag{7}$$

– the covariance matrix of coordinate estimates $\Sigma_{\widehat{C}_j} = s_0^2 \mathbf{Q}_{\widehat{C}_j}$:

$$\Sigma_{\widehat{C}_j}_{(15,15)} = \begin{pmatrix} \Sigma_{\widehat{C}1} & \Sigma_{\widehat{C}12} & \cdots & \cdots & \Sigma_{\widehat{C}15} \\ \Sigma_{\widehat{C}21} & \Sigma_{\widehat{C}2} & & & \\ \vdots & & \Sigma_{\widehat{C}3} & & \vdots \\ \vdots & & & \Sigma_{\widehat{C}4} & \\ \Sigma_{\widehat{C}51} & & \cdots & & \Sigma_{\widehat{C}5} \end{pmatrix} =$$

$$\begin{pmatrix} s_{\widehat{X}1}^2 & s_{\widehat{X}1\widehat{Y}1} & s_{\widehat{X}1\widehat{Z}1} & s_{\widehat{X}1\widehat{X}2} & s_{\widehat{X}1\widehat{Y}2} & s_{\widehat{X}1\widehat{Z}2} & \cdots & & \\ s_{\widehat{Y}1\widehat{X}1} & s_{\widehat{Y}1}^2 & s_{\widehat{Y}1\widehat{Z}1} & s_{\widehat{Y}1\widehat{X}2} & s_{\widehat{Y}1\widehat{Y}2} & s_{\widehat{Y}1\widehat{Z}2} & & & \\ s_{\widehat{Z}1\widehat{X}1} & s_{\widehat{Z}1\widehat{Y}1} & s_{\widehat{Z}1}^2 & s_{\widehat{Z}1\widehat{X}2} & s_{\widehat{Z}1\widehat{Y}2} & s_{\widehat{Z}1\widehat{Z}2} & & & \\ & & & s_{\widehat{X}2}^2 & s_{\widehat{X}2\widehat{Y}2} & s_{\widehat{X}2\widehat{Z}2} & & & \\ \vdots & & & s_{\widehat{Y}2\widehat{X}2} & s_{\widehat{Y}2}^2 & s_{\widehat{Y}2\widehat{Z}2} & & & \\ & & & s_{\widehat{Z}2\widehat{X}2} & s_{\widehat{Z}2\widehat{Y}2} & s_{\widehat{Z}2}^2 & & & \\ & & & & & & \Sigma_{\widehat{C}3} & & \\ & & & & & & & \Sigma_{\widehat{C}4} & \\ & & & & & & & & \Sigma_{\widehat{C}5} \end{pmatrix}. \quad (8)$$

3.3. Quality of new determining points in LGN

For the points established and measured in the ETRS system $B_j (j = 1, 2, 3, 4, 5)$ for LGN, it is necessary to assess their real geometric and functional qualities. Those qualities are mainly characterized by the dimensions and shape of the appropriate closed ellipsoidal point confidence region (CR), which includes points B_j.

For each determined point (Fig. 3) $B_j(X, Y, Z)^E$ – "Remote", concerning the point $A_i(X, Y, Z)^{E,U}$ – "Base" in LGN, the position, shape, and size of the CR of the determined point B_j are created based on the taken measurements.

In the illustrated situation for the determination of points $B_j(X, Y, Z)^E$ to points $A_i(X, Y, Z)^{E,U}$, their $\mathbf{C^{ETRS}}$ determined by GNSS observations in LGN:

- $A_i(X, Y, Z)^{E,U}$ – real points with known coordinates in systems: $\mathbf{C_{Ai}^{ETRS}}$ and $(\mathbf{C_{Ai}^{UTCN}}, \mathbf{H_{Ai}^{BVD}})$;
- $B_j(X, Y, Z)^E$ – new, established point in LGN;
- $B_j(\widehat{X}, \widehat{Y}, \widehat{Z})^E$ – the actual 3D coordinate position of the mark B_j when taking into account errors $\varepsilon_X, \varepsilon_Y, \varepsilon_Z$ in coordinates, i.e. concerning the physical place of
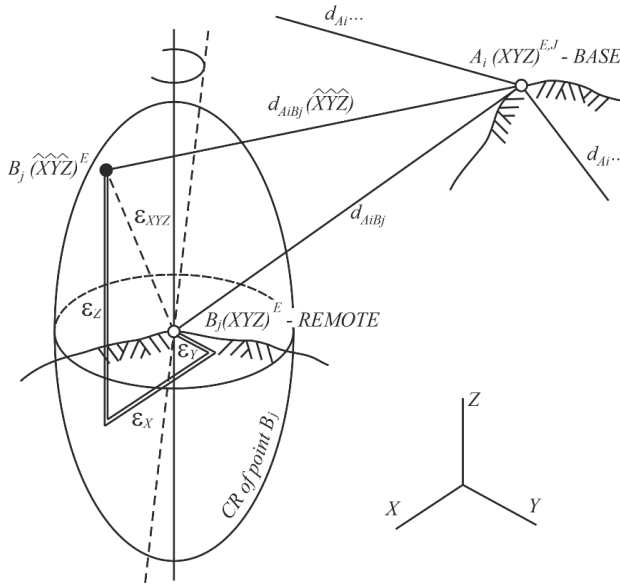
Fig. 3. Determination of points $B_j (X, Y, Z)^E$ from points $A_i (X, Y, Z)$

the point $B_j(X, Y, Z)^E$ around which the appropriate 3D CR is created with the selected confidence α;

– $d_{AiBj(\widehat{X}\widehat{Y}\widehat{Z})}$ – length of the vector from a point A_i to B_j which creates the real position of a point $B_j(\widehat{X}, \widehat{Y}, \widehat{Z})^E$, determined from measurements;

– ε_{XYZ} – fictitious virtual point $B_j(\widehat{X}, \widehat{Y}, \widehat{Z})^E$ deflected from the position of the point $B_j(X, Y, Z)^E$ by errors $\varepsilon_X, \varepsilon_Y, \varepsilon_Z$.

For the position of points $B_j(X, Y, Z)^E$, various CRs with localization points $B_j(X, Y, Z)^E$ can generate from measurements in the LGN field, which are the actual positions B_j with a probability of $1 - \alpha$ (selected value). Standard deviations $\pm(s_{\widehat{X}}, s_{\widehat{Y}}, s_{\widehat{Z}})$ of point coordinates $B_j(X, Y, Z)$ geometrically determine the 3D closed areas around the determined points B_j. These closed areas can be rectangle blocks with dimensions $2s_{\widehat{X}} \times 2s_{\widehat{Y}} \times 2s_{\widehat{Z}}$ around the corresponding point $\widehat{C}_j(\widehat{X}, \widehat{Y}, \widehat{Z})$, respectively with dimensions $2s_{\widehat{X}}\sqrt{F_{1,n-k,\alpha}} \times 2s_{\widehat{Y}}\sqrt{F_{1,n-k,\alpha}} \times 2s_{\widehat{Z}}\sqrt{F_{1,n-k,\alpha}}$, if we consider the $(1 - \alpha)$ probability confidence interval. It creates CRs from a functional perspective, i.e., geometric areas of various ellipsoidal and other geometric structures for points $B_j(X, Y, Z)$ with reliability at a chosen level of significance. The smaller 3D ellipsoidal CRs will assign to points B_j, the more precise (reliable) the coordinates $\widehat{C}_j(\widehat{X}, \widehat{Y}, \widehat{Z})$ of the newly established points B_j will be.

Based on the obtained coordinate estimates and their standard deviations ($\widehat{X} \pm s_{\widehat{X}}$, $\widehat{Y} \pm s_{\widehat{Y}}, \widehat{Z} \pm s_{\widehat{Z}})_j$, it is possible and suitable to create various CRs from the probabilistic positions (Leick, 2004; Jager et al., 2005; Sokol et al., 2014; Xu, 2007; Hoffmann-

Wellenhof et al., 2008). Various analyses of measurements and evaluation of their results are obtained from the multiple possibilities for assessing the quality of points B_j determined by GNSS technology. The complex expression describing the accuracy of an estimated point $\widehat{C}_j(\widehat{X}, \widehat{Y}, \widehat{Z})$ in 3D space from its 3×3 covariance matrix $\boldsymbol{\Sigma}_{\widehat{C}j} = s_0^2 \mathbf{Q}_{\widehat{C}j}$ (Eq. (7)) is represented graphically by its confidence (error) ellipsoid, generally known by its equation (Caspary, 2000; Leick, 2004)

$$(\mathbf{C} - \widehat{\mathbf{C}_j})^T \mathbf{Q}_{\widehat{\mathbf{C}_j}}^{-1} (\mathbf{C} - \widehat{\mathbf{C}_j}) = 3s_0^2 F_{1-\alpha, 3, n-k}, \tag{9}$$

which in the orthogonal coordinate system of eigenvectors z_{e1}, z_{e2}, z_{e3}, belonging to the decreasing magnitudes of the eigenvalues $\lambda_1 \geqslant \lambda_2 \geqslant \lambda_3$ takes the form:

$$\frac{z_{e1}^2}{a^2} + \frac{z_{e2}^2}{b^2} + \frac{z_{e3}^2}{c^2} = 1, \tag{10}$$

with lengths of principal axes:

$$a, b, c = s_0 \sqrt{3\lambda_i F_{1-\alpha, 3, n-k}}, \quad i = 1, 2, 3, \tag{11}$$

where λ_1, λ_2, λ_3 are the eigenvalues of the matrix $\mathbf{Q}_{\widehat{C}j}$. The directions of the principal axes are given by the eigenvectors belonging to the columns of the matrix $\mathbf{X}$:

$$diag(\lambda_i) = \mathbf{X}^{-1} \mathbf{Q}_{\widehat{C}j} \mathbf{X}. \tag{12}$$

After measuring new points B_j ($j = 1, 2, 3, 4, 5$) and taking into account their official data (GCCA of SR, Survey control point data, National spatial network, i.e. 3D accuracy of existing reference points A_i ($i = 1, 2, 3$)), the quality of the point network in LS will be characterized by, for example, the size and formation of ellipsoidal CRs.

Deformation networks are established for specific purposes according to a carefully designed project, in which it is defined, among other things: coordinate system (local or national), reduction of measurements to processable space (i.e., to the appropriate coordinate system), accuracy requirements, observation methodology and measurement processing etc. For these purposes, the mean coordinate error (root mean square error) in the project was set at 2.5 mm. For various reasons (measurement with limited visibility to the sky, or with a reduced number of satellites, etc.), there may be a situation where some points do not meet this condition and cannot be used for these purposes. It is necessary to increase the accuracy of the determination of these points by repeating the measurement of non-compliant points under changed satellite constellation so that they meet the precision condition of the usability of LGN points for deformation purposes. Consequently, such points can also be used for the transformation process: $\mathbf{C}^{\mathbf{ETRS}} \rightarrow \mathbf{C}^{\mathbf{UTCN}}$ and $\mathbf{H}^{\mathbf{BVD}}$.

In the structure created by the LGN, its point field will consist of:

– existing reference points A_i with their known CRs from the documentation of GCCA SR: "Survey control point data, National spatial network";

– new points B_j ($j = 1, 2, 3, 4, 5$) determined by GNSS technology which, also with a posteriori standard coordinate deviations as well as confidence parameters, characterize the positions of points B_j and their a posteriori conditions and properties.

Apart from the visual assessment of the ellipsoidal regions of points B_j, it is also necessary to determine their CRs using appropriate mathematical methods. By depending upon the results, we use only those points B_j in LS that are suitable in terms of their quality.

4. Transformation of coordinates – $\hat{\mathbf{C}}^{\mathbf{ETRS}}$ of points $\mathbf{B_j}$ to coordinates $\mathbf{C}^{\mathbf{UTCN(tr)}}$ and $\mathbf{H}^{\mathbf{BVD(tr)}}$

The ETRS coordinates $\widehat{\mathbf{C}}_{\mathbf{Bj}} = \left(\widehat{X} \pm s_{\widehat{X}}, \widehat{Y} \pm s_{\widehat{Y}}, \widehat{Z} \pm s_{\widehat{Z}} \right)_j$, of the newly established points B_j ($j = 1, 2, 3, 4, 5$) calculated from the result of the GNSS measurements in LGN. All points A_i, or only some, reliable points from this group, will be used for this transformation. The selected points A_i for the transformation $B_j(ETRS) \rightarrow B_j(UTCN, BVD)$ should also create a suitable configuration with determined points B_j that enter into the transformation $B_j(ETRS) \rightarrow B_j(UTCN, BVD)$ with their coordinates.

From various proper transformation methods verified for local situations and conditions (Hefty and Frohmann, 1998; Melicher and Flassik, 1998; Fukushima, 1999; Leick, 2004; Hoffmann-Wellenhof et al., 2008; Thaller et al., 2011), any transformation process with a determination of the values $\mathbf{C}_{\mathbf{Bj}}^{\mathbf{UTCN(tr)}}$, $\mathbf{H}_{\mathbf{Bj}}^{\mathbf{BVD(tr)}}$ and their covariance characteristics will apply for the transformation $\widehat{\mathbf{C}}_{\mathbf{Bj}}^{\mathbf{ETRS}} \rightarrow (\mathbf{C}_{\mathbf{Bj}}^{\mathbf{UTCN}}, \mathbf{H}_{\mathbf{Bj}}^{\mathbf{BVD}})$. With such applicability, the transformation models of Kravinsky–Thompson, Veis, Molodensky–Badekas, Bursa–Wolf, Vancik, also adaptable for nonstandard, more complicated local conditions, are known.

Based on empirically verified application methods regarding the transformation of coordinates $\widehat{\mathbf{C}}_{\mathbf{Bj}}^{\mathbf{ETRS}} \rightarrow (\mathbf{C}_{\mathbf{Bj}}^{\mathbf{UTCN(tr)}}, \mathbf{H}_{\mathbf{Bj}}^{\mathbf{BVD(tr)}})$ in small, local areas, the transformation models of Molodensky–Badekas as well as Bursa–Wolf are mainly used, with suitable, additional modifications (Niemeier, 2002; Leick, 2004; Jager et al., 2005; Hoffmann-Wellenhof et al., 2008).

Every model of transformation of coordinates from ETRS to D-UTCN and BVD-AA in its full range also includes all "partial" transformations, the output of which creates the necessary data for their use in the basic transformation process. In this model, the ETRS coordinates of the point B_j will change to the coordinates of positions and heights in the D-UTCN and BVD-AA systems.

To use LGN points for deformation purposes in the D-UTCN coordinate system, it is necessary to transform not only the 3D coordinates of the ETRS89 coordinate system into a 2D projection coordinate system D-UTCN, but also their accuracy characteristics. The calculation can be formally divided into two steps:

1. Transformation of Cartesian coordinates from ellipsoid GRS80 to ellipsoid Bessel 1841 is by means of 7-parameter Helmert transformation, called three-dimensional

conformal transformation – Bursa Wolf's model (Droscak, 2018) in matrix form:

$$\mathbf{C}^{\mathbf{Bessel}} = \mathbf{T} + (1 + m)\mathbf{R}\ \mathbf{C}^{\mathbf{ETRS}}, \tag{13}$$

or

$$\begin{pmatrix} X \\ Y \\ Z \end{pmatrix}^{\mathbf{Bessel}} = \begin{pmatrix} T_X \\ T_Y \\ T_Z \end{pmatrix} + (1 + m)\begin{pmatrix} 1 & r_Z & -r_Y \\ -r_Z & 1 & r_X \\ r_Y & -r_X & 1 \end{pmatrix}\begin{pmatrix} X \\ Y \\ Z \end{pmatrix}^{\mathbf{ETRS}}, \tag{14}$$

where $\mathbf{T}$ is the translation vector in the direction of the individual axes, $\mathbf{R}$ is the rotation matrix and m is the scaling parameter. Due to the compatibility of geodetic works, all 7 parameters of the transformation key are determined by Decree of GCCA SR no. 300/2009 Coll.

The transformation of covariance matrices of spatial coordinates is performed according to:

$$\mathbf{\Sigma}_{\mathbf{C}}^{\mathbf{Bessel}} = \mathbf{R}\ \mathbf{\Sigma}_{\mathbf{C}}^{\mathbf{ETRS}}\ \mathbf{R}; \tag{15}$$

2. The transformation of Cartesian coordinates from the Bessel 1841 ellipsoid to positional cartographic coordinates in the D-UTCN coordinate system (Krovak's projection) consists of a sequence of generally known transformations:

$$\begin{pmatrix} X \\ Y \\ Z \end{pmatrix}^{\mathrm{Bessel}} \Rightarrow \begin{pmatrix} \varphi \\ \lambda \\ h \end{pmatrix}^{\mathrm{Bessel}} \Rightarrow \begin{pmatrix} U \\ V \end{pmatrix}^{\mathrm{Gauss}} \Rightarrow \begin{pmatrix} \check{S} \\ D \end{pmatrix} \Rightarrow \begin{pmatrix} R \\ D \end{pmatrix} \Rightarrow \begin{pmatrix} x \\ y \end{pmatrix}^{\mathrm{UTCN}}, \tag{16}$$

where: $(X\ Y\ Z)^T$ – Cartesian coordinates on the Bessel ellipsoid;
$\quad\quad\quad (\varphi\ \lambda\ h)^T$ – ellipsoidal coordinates and geodetic (ellipsoidal) height;
$\quad\quad\quad (U\ V)^T$ – spherical coordinates on a Gaussian sphere;
$\quad\quad\quad (\check{S}\ D)^T$ – cartographic coordinates;
$\quad\quad\quad (R\ D)^T$ – polar coordinates on the oblique cone surface;
$\quad\quad\quad (x\ y)^T$ – positional coordinates in the D-UTCN coordinate system.

Orthometric height H^{BVD} in BVD-AA is determined from ellipsoidal height h by adding the height of the Digital Height Reference Model (DVRM). Transformations of the relevant covariance matrices are performed according to Gasinec et al. (2019).

For points B_j from the transformation of their coordinates $\widehat{\mathbf{C}}_{\mathbf{Bj}}^{\mathbf{ETRS}}$ to coordinates $\mathbf{C}_{\mathbf{Bj}}^{\mathbf{UTCN(tr)}}$, $\mathbf{H}_{\mathbf{Bj}}^{\mathbf{BVD(tr)}}$, we obtain data regarding coordinates as well as BVD-AA heights

and their covariance structures in the D-UTCN and BVD-AA systems:

$$
\mathbf{C}_{\mathbf{Bj}}^{\mathbf{UTCN(tr)}} = \begin{pmatrix} B_1(x_1y_1) \\ B_2(x_2y_2) \\ B_3(x_3y_3) \\ B_4(x_4y_4) \\ B_5(x_5y_5) \end{pmatrix},
$$

$$
\boldsymbol{\Sigma}_{\mathbf{C_{Bj}}}^{\mathbf{UTCN(tr)}} = \left(\begin{array}{cc|cc|c|c}
s_{x1}^2 & s_{x1y1} & s_{x1x2} & s_{y1y2} & \cdots & \cdots \\
s_{y1x1} & s_{y1}^2 & s_{y2y1} & s_{y1y2} & & \\ \hline
& & s_{x2}^2 & s_{x2y2} & & \\
& & s_{y2x2} & s_{y2}^2 & & \\ \hline
\vdots & & & & \ddots & \\ \hline
\vdots & & & & & \ddots \\ \hline
& & & & & s_{x5}^2 \quad s_{x5y5} \\
& & & & & s_{y5x5} \quad s_{y5}^2
\end{array} \right),
\tag{17}
$$

$$
\mathbf{H}_{\mathbf{Bj}}^{\mathbf{BVD(tr)}} = \begin{pmatrix} B_1(H_1) \\ B_2(H_2) \\ B_3(H_3) \\ B_4(H_4) \\ B_5(H_5) \end{pmatrix},
$$

$$
\boldsymbol{\Sigma}_{\mathbf{H_{Bj}}}^{\mathbf{BVD(tr)}} = \left(\begin{array}{c|c|c|c|c}
s_{H1}^2 & s_{H1H2} & \cdots & \cdots & \\ \hline
s_{H2H1} & s_{H2}^2 & & & \\ \hline
\vdots & & \ddots & & \\ \hline
\vdots & & & \ddots & \\ \hline
& & & & s_{H5}^2
\end{array} \right).
\tag{18}
$$

Based on the proposed methods or the use of other suitable, verified transformations, coordinates $\widehat{\mathbf{C}}^{\mathbf{ETRS}}(X, Y, Z)$, as well as coordinates $\mathbf{C}^{\mathbf{UTCN(tr)}}(x, y)$ and $\mathbf{H}^{\mathbf{BVD(tr)}}(H_j)$, together with appropriate parameters of their quality, will be obtained for all points A_i, B_j in the LGN. With the obtained coordinates and height, points A_i, B_j will provide the quality of geodetic, planimetric, and vertical structure of the LGN and the reliable geodetic implementation of building works.

5. Results and discussion

At points A_i ($i = 1, 2, 3$) and B_j ($j = 1, 2, 3, 4, 5$) in the LGN (Fig. 1), observations were realized by Leica GNSS receivers. Coordinates of the points A_i fixed during the processing of observations using the company software of GNSS receiver and the approximate reduced coordinates $\mathbf{C}^{\circ\mathbf{ETRS\_Red}}$ of LGN points were obtained (Table 1). By subsequent processing using the GMM of full rank adjustment procedure, the estimates of the complements of the adjusted reduced coordinates $\mathbf{d\widehat{C}}^{\mathbf{ETRS\_Red}}$ (Table 1), together with estimates of the adjusted, reduced coordinates $\mathbf{\widehat{C}}^{\mathbf{ETRS\_Red}}$ (Eq. (4)) of LGN points, were obtained. The accuracy of the coordinate estimates $\mathbf{s}_{\widehat{\mathbf{C}}}^{\mathbf{ETRS\_Red}}$ were obtained as the square root of the main diagonal of the covariance matrix $\mathbf{s}_{\widehat{\mathbf{C}}}^{\mathbf{ETRS\_Red}} = \mathrm{sqrt}\left(\mathrm{diag}\mathbf{\Sigma}_{\widehat{\mathbf{C}}}^{\mathbf{ETRS\_Red}}\right)$ (Eq. (12)) (Table 1).

Based on the results of processing, the visualization of LGN using the estimates of adjusted coordinates $\mathbf{\widehat{C}}^{\mathbf{ETRS\_Red}}$ from the adjustment, was done. 3D ellipsoids based on the corresponding covariance submatrices $\mathbf{\Sigma}_{\widehat{\mathbf{C}}}^{\mathbf{ETRS\_Red}}$ of individual points (where accuracies of coordinate estimates $\mathbf{s}_{\widehat{\mathbf{C}}}^{\mathbf{ETRS\_Red}}$ lie on their diagonals) plotted at the points of LGN. The orientation of LGN visualization in the ETRS coordinate system is in a general position (Fig. 1 vs. Fig. 4).
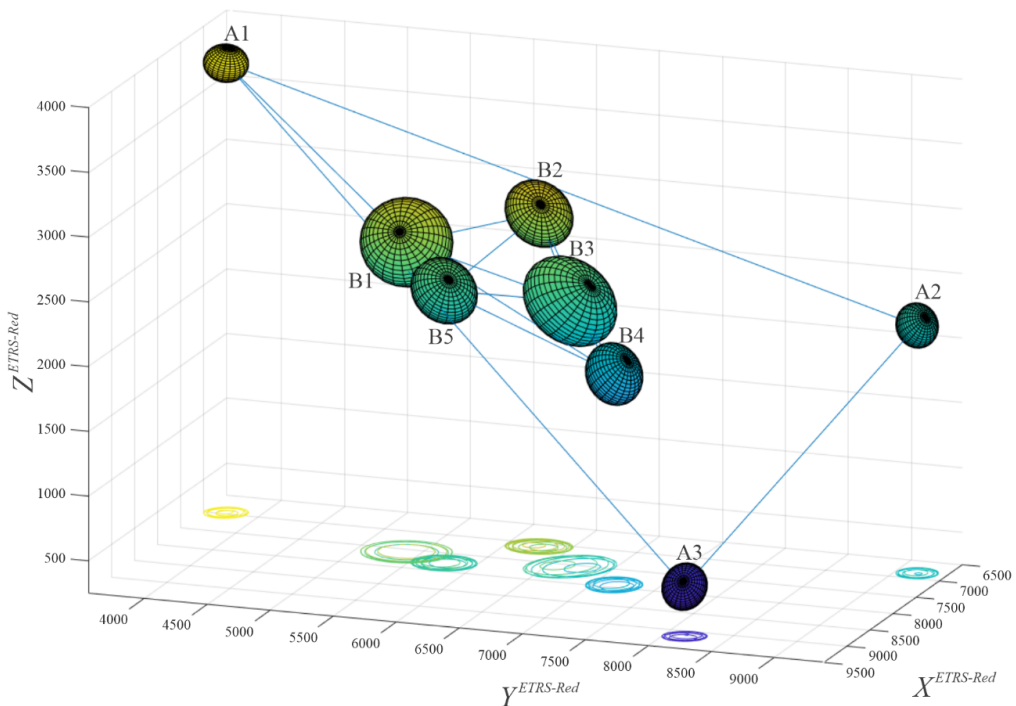

Fig. 4. 3D CR of reference existing points A_i and newly established points B_j in ETRS

Table 1. Estimates of reduced LGN parameters

Point		$C°^{ETRS\_Red}$ (m)	$d\widehat{C}^{ETRS\_Red}$ (mm)	$\widehat{C}^{ETRS\_Red}$ (m)	$s_{\widehat{C}}^{ETRS\_Red}$ (mm)
A_1	X	6968.7516	−1.39	6968.7502	0.58
	Y	3728.4934	1.38	3728.4948	0.57
	Z	3720.4321	1.22	3720.4333	0.41
A_2	X	6844.4725	1.36	6844.4739	0.55
	Y	9171.0417	−1.34	9171.0402	0.53
	Z	2162.8451	−1.39	2162.8437	0.58
A_3	X	9145.9863	−1.21	9145.9851	0.40
	Y	8162.5368	1.41	8162.5383	0.60
	Z	633.1741	−1.44	633.1727	0.63
B_1	X	7568.3825	1.69	7568.3842	2.01
	Y	5379.9851	−2.25	5379.9828	2.57
	Z	2640.7553	2.02	2640.7573	2.34
B_2	X	7086.3572	1.66	7086.3589	1.05
	Y	6257.1481	−1.94	6257.1462	1.33
	Z	2820.2208	1.89	2820.2227	1.28
B_3	X	7552.1627	2.37	7552.1651	2.69
	Y	6672.8531	−1.81	6672.8513	2.13
	Z	2299.2297	2.04	2299.2317	2.36
B_4	X	7932.6129	−1.72	7932.6112	1.11
	Y	7161.4672	−1.58	7161.4656	0.97
	Z	1878.2387	1.67	1878.2404	1.06
B_5	X	7774.4315	1.72	7774.4332	1.11
	Y	5754.1288	1.95	5754.1307	1.34
	Z	2352.7349	−1.89	2352.7330	1.28

The use of such a LGN in the risk area is widely used, especially for environmental protection, population safety, asset and industrial protection, and the sustainable development of human society.

When assessing points B_j, apart from the analytical assessment of the quality of their confidence properties (shape, size, position), it is also suitable to apply their empirical evaluation in the structure of the given point field. If GNSS observations are without potential gross errors and outliers, the LSM provides the best results. Otherwise, robust methods such as Robust M – estimates by Huber or Hampel (Labant et al., 2014) should be used. In the given LGN (Fig. 4) points B_1, B_3 with their confidence conditions are assessed visually together with appropriate mathematical criteria. Based on the accuracy

of the point coordinates estimation (Table 1), it is evident that points B_1 and B_3 have the lowest accuracy compared to the accuracies of other points.

To compare and evaluate the quality of the LGN points, a means spatial error on j-th LGN point s_{3Dj} or average means spatial error of all LGN points s_{3D} determined from the main diagonal of the coordinate matrix of adjusted coordinates $\mathbf{s}_{\widehat{C}}^{\mathbf{ETRS\_Red}}$ (Table 1) in the general form can use:

$$s_{3Dj} = \sqrt{s_{\widehat{X}j}^2 + s_{\widehat{Y}j}^2 + s_{\widehat{Z}j}^2} \quad \text{or} \quad s_{3D} = \frac{\sum_{j=1}^{b} \sqrt{s_{\widehat{X}j}^2 + s_{\widehat{Y}j}^2 + s_{\widehat{Z}j}^2}}{b}, \tag{19}$$

where b is the number of points for calculating s_{3D}.

The maximum mean spatial error is at point B_3 and has a value of $s_{3D_3} = 4.16$ mm. The average mean spatial error for reference (existing) points A_i, $i = 1, 2, 3$ is $s_{3D_A} = 0.95$ mm, for all established LGN points B_j is $s_{3D_B} = 2.86$ mm.

The use of LGN points B_j for deformation purposes must be verified by meeting the condition of the mean coordinate error (root mean square error) = 2.5 mm, the value of which is defined in the deformation analysis project. The mean coordinate error on $j - th$ LGN point s_{XYZj} and the average mean coordinate error of all LGN points s_{XYZ} are determined by:

$$s_{XYZj} = \sqrt{\frac{s_{\widehat{X}j}^2 + s_{\widehat{Y}j}^2 + s_{\widehat{Z}j}^2}{3}} = \frac{s_{3Dj}}{\sqrt{3}} \quad \text{or} \quad s_{XYZ} = \frac{\sum_{j=1}^{b} s_{XYZj}}{b}. \tag{20}$$

The maximum mean coordinate error is at point B_3 and has a value of 2.40 mm. Based on which it is possible to confirm that all established points B_j meet the condition of serviceability < 2.5 mm for deformation purposes. The average mean coordinate error for all reference points A_i is $s_{XYZ_A} = 0.54$ mm and for all establised points B_j is $s_{XYZ_B} = 1.65$ mm.

The same conclusion is found in the statistical testing of the quality control of the determination of the point coordinates estimation, i.e. that points B_2, B_4 and B_5 determined with higher accuracy than points B_1 and B_3. The same conclusion about the quality of LGN points represented by their visualization (Fig. 4), where the largest 3D ellipsoids are visualized at points B_1, B_3. As all points meet the accuracy condition of the points determination defined in the deformation project, they can be transformed into D-UTCN and BVD-AA, according to the transformation procedure given in section 4. For various reasons, some points may not meet this condition and cannot be used for strain analysis. Then it is necessary to increase the accuracy of determining these points by repeating the measurement of unsatisfactory points with a changed distribution of satellites in orbit or by including new GNSS baseline vectors in the observation vector. And then it is necessary to perform repeated LSM adjustments with updated input data.

The transformation results of the LGN points from the 3D coordinate system ETRS to the 2D coordinate system D-UTCN and vertical datum BVD-AA were reduced and shown in Table 2. The visualization of the transformation results $\left(\mathbf{C^{UTCN\_Red(tr)}}\right.$ and $\mathbf{H^{BVD\_Red(tr)}}\left.\right)$ in the D-UTCN coordinate system using standard error ellipses in the cartographic plane of the Krovak's projection and in the BVD-AA vertical system using standard deviations of normal (Molodensky's) heights (Fig. 5).

Table 2. Transformed reduced coordinates of points of LGN in D-UTCN and heights in BVD-AA

Point	$\mathbf{C^{UTCN\_Red(tr)}}$ (m)		s_C^{UTCN} (mm)	$\mathbf{H^{BVD\_Red(tr)}}$ (m)	s_H^{BVD} (mm)
A_1	x	4907.178	0.51	251.578	0.58
	y	5566.003	0.53		
A_2	x	7566.330	0.49	307.098	0.60
	y	568.010	0.56		
A_3	x	9826.963	0.46	330.368	0.65
	y	2449.545	0.55		
B_1	x	6549.098	2.22	203.218	2.41
	y	4319.669	2.49		
B_2	x	6378.651	1.11	251.791	1.29
	y	3318.519	1.26		
B_3	x	7171.098	2.55	245.928	2.39
	y	3136.767	2.19		
B_4	x	7862.403	1.09	280.319	1.11
	y	2851.314	1.01		
B_5	x	6997.614	1.18	202.861	1.34
	y	4066.357	1.30		

All LGN points B_j can suitably use for very precise geodetic activities. For example, geodetic monitoring of the stability of populated area for population security and property protection (Kukucka, 2013), geodetic monitoring of the stability of building structure to protect the environment, property, and industry (Labant, 2013; Labant et al., 2014), deformation monitoring of the stability of industrial zones for the long-term sustainable development of human society and the prevention of its devastation (Kolcun and Sutti, 2000; Tzenkov and Gospodinov, 2003). From long-term geodetic monitoring using analyses and forecasts, it is possible to predict the future stability or instability development of the already monitored area, building site, or industrial zones.
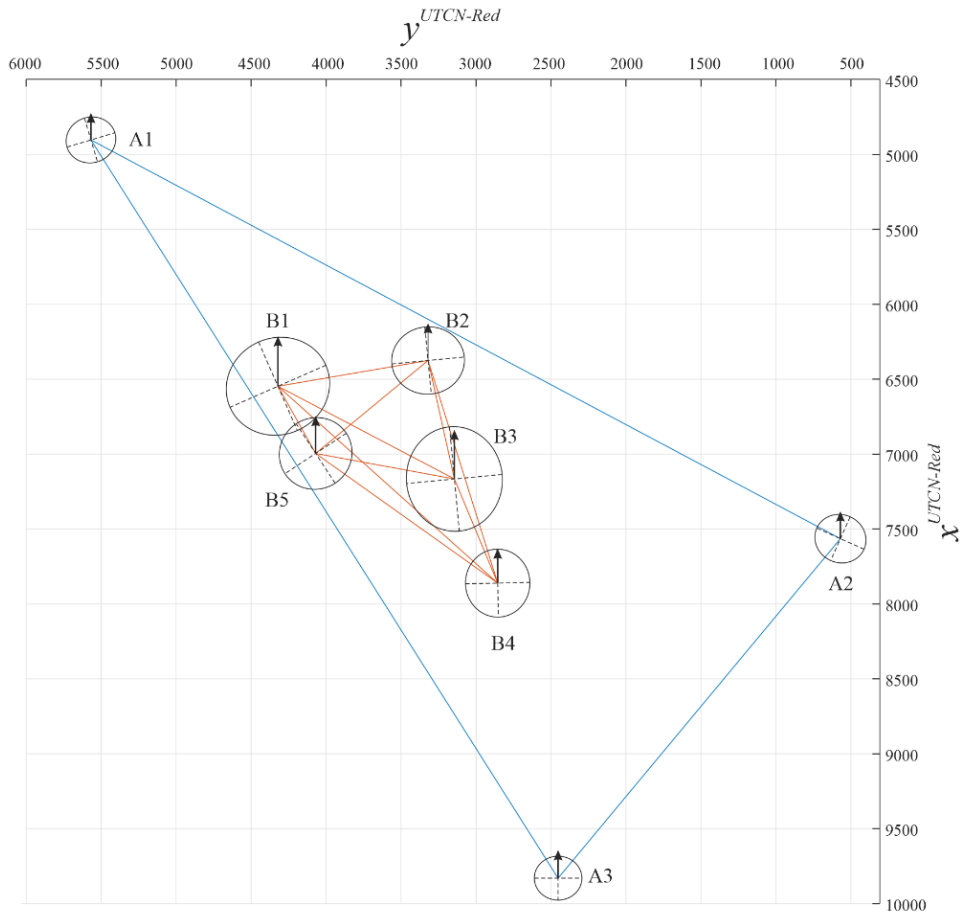
Fig. 5. Standard error ellipses and standard deviations of existing reference points A_i and newly established points B_j in D-UTCN and BVD-AA

6. Conclusions

The submitted manuscript concerns the necessary geodetic practice with various tasks, intentions, and objectives for building or subsequent observation of various objects and areas in LS. Long-term monitoring provides high-quality outputs that are important for environmental protection, population safety, and human society's sustainable development. For the implementation of such tasks and objectives across SR, in various locations, it is possible to establish and use the required survey control points with coordinates from both coordinate systems: $\mathbf{C}^{\mathbf{UTCN}}(x, y)$, $\mathbf{H}^{\mathbf{BVD}}(H)$, and also $\mathbf{C}^{\mathbf{ETRS}}(X, Y, Z)$. The common objective is to add the necessary geodetic points into the existing LGN. These new points are essential regarding the required quality of building work.

This manuscript includes the necessary preconditions and methods so that the implementation of geodetic objectives and steps in a given LS will provide the creation of

required and suitable point fields in the ETRS and D-UTCN with precision coordinate estimates, and in the BVD-AA with appropriate heights.

In this study based on GNSS observations at LGN points, the coordinates estimate of newly established points B_j were determined using LSM adjustment. Based on the accuracy of the coordinate estimate, the mean coordinate error was determined for each established point B_j. All points have met the condition defined in the project and are applicable for the purposes defined in the project. Subsequently, the coordinates were transformed into the national systems D-UTCN and BVD-AA.

The results of deformation analysis can provide decisive conclusions. Early signaling can inform of impending dangers that may impact the reduction of economic damage and the increase of human safety, the stability of sustainable social development, and environmental protection. The population will feel much safer in the monitored area. Early detection of imminent dangers will prevent a natural disaster with losses on human life, damage to property, and environmental devastation. These effects have an impact on the environmental, economic, and social pillars of the sustainable development of human society.

Author contributions

Conceptualization: G.W. and S.L.; methodology: G.W., S.L. and J.G.; software: S.L.; validation: S.L., H.S. and P.C.; formal analysis: H.S., P.C., E.W. and R.W.; investigation: G.W. and S.L.; resources: S.L., E.W. and R.W.; data curation: S.L. and J.G.; writing – original draft preparation: G.W. and S.L.; writing – review and editing: S.L. and J.G.; visualization: S.L.; supervision: S.L.

Data availability statement

The data used to support the findings of this study are available from the corresponding author upon reasonable request.

Acknowledgements

References

Bakon, M., Oliveira, I., Perissin, D. et al. (2017). A Data Mining Approach for Multivariate Outlier Detection in Postprocessing of Multitemporal InSAR Results. *IEEE J. Sel. Top. Appl. Earth Obs. Remote Sens.*, 10(6), 2791–2798. DOI: 10.1109/JSTARS.2017.2686646.

Banas, M., and Ligas, M. (2014). Empirical tests of performance of some M – estimators. *Geod. Cartogr.*, 63(2), 127–146. DOI: 10.2478/geocart-2014-0010.

Baum, R., and Godt, J. (2010). Early warning of rainfall-induced shallow landslides and debris flows in the USA. *Landslides*, 7(3), 259–272. DOI: 10.1007/s10346-009-0177-0.

Capparelli, G., and Tiranti, D. (2010). Application of the MoniFLaIR early warning system for rainfall-induced landslides in Piedmont region (Italy). *Landslides*, 7(4), 401–410. DOI: 10.1007/s10346-009-0189-9.

Caspary, W.F. (2000). *Concepts of network and deformation analysis*. The University of New South Wales, Kensington (Australia).

Decree of GCCA SR no. 300/2009 Coll. implementing the Act of the National Council of the Slovak Republic no. 215/1995 Coll. on geodesy and cartography as amended.

Droscak, B. (2018). Coordinate system of the unified trigonometric cadastral network and its relation to the European Terrestrial Reference System 1989. Technical report. Bratislava, Geodetic and Cartographic Institute Bratislava. Retrieved January 10, 2022, from https://www.geoportal.sk/files/gz/etrs89_s-jtsk_tech_sprava_2014_ver1_0.pdf.

Drabikova, E. (2016). *Project Management from Benefits Perspective*. MMK 2016, Magnanimitas, Hradec Králové, 25–30. DOI: https://doi.org/10.17973/MMSJ.2018_03_201733.

Fukushima, T. (1999). Fast Transform from geocentric to geodetic coordinates. *J. Geod.*, 73(11), 603–610. DOI: 10.1007/s001900050271.

Gasincova, S., and Gasinec, J. (2010). Adjustment of positional geodetic networks by unconventional estimations. *Acta Montan. Slovaca*, 15(1), 71–85. ISSN 1335-1788.

Gasinec, J., and Gasincova, S. (2016). Landslide Deformation Analysis Based on Robust M-estimations. *J. of the Polish Mineral Eng. Soc.*, 17(1), 171–176.

Gasinec, J., Gasincova, S., Stankova, H. et al. (2019). *Observation of horizontal displacements on water structures via GNSS*. In Satellite methods in geodesy and real estate of cadaster. Brno: ECON publishing, s.r.o., p. 85–94, ISBN 978-80-86433-72-1.

Ge, L., Chang, H.C., and Rizos, C. (2007). Mine subsidence monitoring using multi-source satellite SAR images. *Photogramm. Eng. Remote Sens.*, 73(3), 259–266. DOI: 10.14358/PERS.73.3.259.

Gergelova, M., Kuzevicova, Z., Kuzevic, S. et al. (2012). GIS as a supporting tool in the process of hydrodynamic modeling on a selected part of a watercourse. *Acta Hydro. Slovaca*, 13(2), 394–403. ISSN 1335-6291.

Grecea, C., Lenciu, I., Dimen, L. et al. (2012). Impact of surveying engineering on the environmental protection problems. *J. Environ. Prot. Ecol.*, 13(1), 352–360. ISSN 1311-5065.

Hampel, F. (1980). Robuste Schätzungen: Ein anwendungsorientierter Überblick. *Biom. J.*, 22(1), 3–21. DOI: 10.1002/bimj.4710220102.

Hefty, J., and Frohmann, E. (1998). Non-linear 3D transformations and its application to coordinate transfer between S-JTSK and ETRS 89. *Geod.Cartogr. Rev.*, 44(6), 121-126. ISSN 1805-7446.

Hefty, J., and Husar, L. (2007). *Sattelite geodesy – Global positioning system*. STU Bratislava.

Hekimoglu, S. (2005). Do robust methods identify outliers more reliably than conventional tests for outliers? *ZFV – Zeitschrift fur Geodasie, Geoinformation und Landmanagement*, 130(3),174-180.

Hoffmann-Wellenhof, B., Lichtenegger, H. and Wasle, E. (2008). *GNSS – Global Navigation Satellite Systems*. Wien: Springer-Verlag. DOI: 10.1007/978-3-211-73017-1.

Hong, M., Kim, J. and Jeong, S. (2018). Rainfall intensity-duration thresholds for landslide prediction in South Korea by considering the effects of antecedent rainfall. *Landslides*, 15(3), 523–534. DOI: 10.1007/s10346-017-0892-x.

Huber, P.J. (1964). Robust estimation of a location parameter. *Ann. Math. Stat.*, 35(1), 73–101. DOI: 10.1214/aoms/1177703732.

Chae, B., Park, H., Catani, F. et al. (2017). Landslide prediction, monitoring and early warning: a concise review of state-of-the-art. *Geosci. J.*, 21(6), 1033–1070. DOI: 10.1007/s12303-017-0034-4.

Chan, F., Chuah, C., Ziegler, A. et al. (2018). Towards resilient flood risk management for Asian coastal cities: Lessons learned from Hong Kong and Singapore. *J. Clean. Prod.*, 187, 576–589. DOI: 10.1016/j.jclepro.2018.03.217.

ITS (International Technical Standard). (2007). Geographic information. Spatial referencing by coordinates. STN EN ISO 19111, Slovak office of standards, metrology and testing, Bratislava.

Jadviscok, P., Ovesna, G., and Konecny, M. (2016). Multipath and its manifestations in the real environment of geodetic practice. *Geod. Cartogr.*, 42(2), 47–52. DOI: 10.3846/20296991.2016.1198573.

Jager, R., Muller, T., Saler, H. et al. (2005). Classical and robust adjustment methods. Wichmann: Heidelberg.

Jing, Z., Wang, J., Zhu, Y. et al. (2018). Effects of land subsidence resulted from coal mining on soil nutrient distributions in a loess area of China. *J. Clean. Prod.*, 177, 350–361. DOI: 10.1016/j.jclepro.2017.12.191.

Kadaj, R. (2016). The combined geodetic network adjusted on the reference ellipsoid – a comparison of three functional models for GNSS observations. *Geod.Cartogr.*, 65(2), 229–257. DOI: 10.1515/geocart-2016-0013.

Kolcun, S., and Sütti, J. (2000). Deformation analysis of the area around Jaslovské Bohunice. *Acta Montan. Slovaca*, 5(1), 71–76. ISSN 1335-1788.

Krarup, T., and Kubik, K. (1983). The Danish method. Experiance and Philosophy. Deutsche Geodätische Kommission, Seminar on Mathematical Models of Geodetic Photogrammetric Point Determination with Regard to Outliers and Systematic Errors, Germany, 131–134.

Kukucka, P. (2013). *The monitoring of landslide area*. Miskolc: Bíbor Publisher.

Labant, S., Weiss, G., and Kukucka, P. (2011). Robust adjustment of a geodetic network measured by satellite technology in the Dargovských Hrdinov suburb. *Acta Mont. Slovaca*, 16 (3), 229–237. ISSN 1335-1788.

Labant, S. (2013). *Deformation analysis of stability area*. Miskolc: Bíbor Publisher.

Labant, S., Weiss, G., Zuzik, J. et al. (2014). Graphical interpretation deformation analysis of stability area using of strain analysis. *Acta Montan. Slovaca*, 19(1), 31–40. ISSN 1335-1788.

Labant, S., Bindzarova Gergelova, M., Kuzevicova, Z., et al. (2020). Utilization of Geodetic Methods Results in Small Open-Pit Mine Conditions: A Case Study from Slovakia. *Minerals*, 10(6), 489. DOI: 10.3390/min10060489.

Leick, A. (2004). *GPS Satellite Surveying*. (3rd edition). Toronto: John Wiley & Sons.

Ma, K., Liu, G., Guo, L. et al. (2020). Deformation and stability of a discontinuity-controlled rock slope at Dagangshan hydropower station using three-dimensional discontinuous deformation analysis. *Int. J. Rock Mech. Min. Sci.*, 130, 104313. DOI: 10.1016/j.ijrmms.2020.104313.

Manap, N., and Voulvoulis, N. (2016). Data analysis for environmental impact of dredging. *J. Clean. Prod.*, 137, 394–404. DOI: 10.1016/j.jclepro.2016.07.109.

Melicher, J., and Flassik, T. (1998). Coordinate Transfromation from the World Geodetic System 1984 into the Local Coordinate System by Non-Linearized Rotation Matrices. *Geod. Cartogr. Rev.*, 44(2), 25–29. ISSN 1805-7446

Niemeier, W. (2002). *Adjustment Calculation*. Berlin: De Gruyter Verlag.

Popa, A., and Palamariu, M. (2012). *Displacement and deformation analysis for hydropower buildings*. In SGEM – 12th International Multidisciplinary Scientific GeoConference and EXPO, Bulgaria, Varna, 723–730. ISSN 1314-2704.

Pu, F., Ma, J., Zeng, D. et al. (2015). Early Warning of Abrupt Displacement Change at the Yemaomian Landslide of the Three Gorge Region, China. *Nat. Hazards Rev.*, 16(4), 04015004. DOI: 10.1061/(ASCE)NH.1527-6996.0000179.

Qian, T., Wu, H., Zhao, G. et al. (2012). Deformation Monitoring and Environmental protection for Deep Foundation Pit Engineering. *Appl. Mech. Mat.*, 204–208, 2970–2973. DOI: 10.4028/www.scientific.net/AMM.204-208.2970.

Sabova, J., and Pukanska, K. (2007). Projekt der Deformationsuntersuchungen. *Acta Montan. Slovaca*, 12 (special 3), 516–519.

Schonemann, E., Becker, M., and Springer, T. (2011). A new Approach for GNSS Analysis in a Multi-GNSS and Multi-Signal Environment. *J. Geod. Sci.*, 1(3), 204–214. DOI: 10.2478/v10156-010-0023-2.

Sokol, S., Bajtala, M., Jezko, J. et al. (2014). Testing the accuracy of determining three-dimensional Cartesian coordinates using the universal measuring station S8 Trimble DR Plus Robotic. *J. of the Polish Mineral Eng. Soc.*, 33 (1), 85–90. ISSN 1640-4920.

Sun, W., Wang, H., and Hou, K. (2018). Control of waste rock-tailings paste backfill for active mining subsidence areas. *J. Clean. Prod.*, 171, 567-579. DOI: 10.1016/j.jclepro.2017.09.253.

Tej, J., Ali Taha V., Sirkova M. et al. (2015). Factors of crisis situations at the level of large urban areas of Slovakia. *Exclusive journal: economy and society and environment*, 3(2), 41–49. ISSN: 1339-4509.

Thaller, D., Dach, R., Seitz, M. et al. (2011). Combination of GNSS and SLR observations using satellite co-locations. *J. Geod.*, 85(5), 257–272. DOI: 10.1007/s00190-010-0433-z.

Tofani, V., Raspini, F., Catani, F. et al. (2013). Persistent scatterer interferometry (PSI) technique for landslide characterization and monitoring. *Remote Sens.*, 5, 1045–1065. DOI: 10.3390/rs5031045.

Tzenkov, T., and Gospodinov, S. (2003). Geometric Analysis of Geodetic Data for Investigation of 3D Landslide Deformations. *Nat. Hazards Rev.*, 4(2), 78–81. DOI: 10.1061/(ASCE)1527-6988(2003)4:2(78).

Wang, W., Chen, Z., and Li, X. (2018). The arrangement of deformation monitoring project and analysis of monitoring data of a hydropower engineering safety monitoring system. *IOP Conference Series: Earth and Environmental Science*, 128, 012006. DOI: 10.1088/1755-1315/128/1/012006.

Weiss, G., and Jakub, V. (2007). The test verification of 3D geodetic points and their changes. *Acta Montan. Slovaca*, 12 (Special 3), 612–616. ISSN 1335-1788.

Weiss, G., Labant, S., Weiss, E. et al. (2009). Establishment of local geodetic nets. *Acta Montan. Slovaca*, 14 (4), 306–313. ISSN 1335-1788.

Weiss, G., Labant, S., Weiss, E. et al. (2010). Detection of erroneous values in the measurement of local geodetic networks. *Acta Montan. Slovaca*, 15(1), 62–70. ISSN 1335-1788.

Weiss, G., Bartos, K., Labant, S. et al. (2018). The identification of incorrectly determined new points in established 2D local geodetic network during deformation monitoring for environmental protection. *J. Clean. Prod.*, 170, 789–796. DOI: 10.1016/j.jclepro.2017.09.179.

Xu, G. (2007). *GPS theory, Algorithms and Applications*. Berlin: Springer.

Yune, C.Y., Jun, K.J., Kim, K.S. et al. (2010). Analysis of slope hazard-triggering rainfall characteristics in Gangwon Province by database construction. *J. Korean Geotech. Soc.*, 26(10), 27–38. ISSN 1229-2427.

Zelenakova, M., Ganova, L., Purcz, P. et al. (2015). Methodology of flood risk assessment from flash floods based on hazard and vulnerability of the river basin. *Nat. Hazards Rev.*, 79 (3), 2055–2071. DOI: 10.1111/jfr3.12298.

Zelenakova, M., Ganova, L., Purcz, P. et al. (2018). Determination of the potential economic flood damages in Medzev, Slovakia. *J.Flood Risk Manag.*, 11(1), 1090–1099. DOI: 10.1007/s11069-015-1945-x.

Zhou, C., Shao, W., and van Westen, C.J. (2014). Comparing two methods to estimate lateral force acting on stabilizing piles for a landslide in the Three Gorges Reservoir, China. *Eng. Geol.*, 173, 41–53. DOI: 10.1016/j.enggeo.2014.02.004.